Available online at www.sciencedirect.com
SCIENCE DIRECT
Journal of Pharmaceutical and Biomedical Analysis 41 (2006) 857–865
JOURNAL OF PHARMACEUTICAL AND BIOMEDICAL ANALYSIS
www.elsevier.com/locate/jpba

Sildenafil/cyclodextrin complexation: Stability constants, thermodynamics, and guest–host interactions probed by ^{1}H NMR and molecular modeling studies

Mahmoud M. Al Omari [a,*], Mohammad B. Zughul [b], J. Eric D. Davies [c], Adnan A. Badwan [a]

[a] *The Jordanian Pharmaceutical Manufacturing Company, Naor, Jordan*
[b] *Department of Chemistry, University of Jordan, Amman, Jordan*
[c] *Department of Environmental Science, Lancaster University, Lancaster, United Kingdom*

Received 24 August 2005; received in revised form 26 January 2006; accepted 29 January 2006
Available online 9 March 2006

Abstract

Guest–host interactions of sildenafil (Sild) with cyclodextrins (CyDs) have been investigated using several techniques including phase solubility diagrams (PSD), differential scanning calorimetry (DSC), X-ray powder diffractometry (XRPD), proton nuclear magnetic resonance (^{1}H NMR) and molecular mechanical modeling (MM$^+$). Estimates of the complex formation constant (K_{11}) show that the tendency of Sild to complex with CyDs follows the order: β-CyD > HP-β-CyD > γ-CyD, α-CyD, where K_{11} values at pH 8.7 and 30 °C were 150, 68 and 46, 43 M^{-1}, respectively. Ionization of Sild reduces its tendency to complex with β-CyD, where protonated (at pH 3.6) and anionic Sild (at pH 12.1) species have K_{11} values of 17 and 42 M^{-1}, respectively, compared with 150 M^{-1} for neutral Sild (at pH 8.7). The hydrophobic character of Sild was found to provide 39% of the driving force for complex stability, while other factors including specific interactions contribute −7.9 kJ/mol. Complex formation of Sild with β-CyD ($\Delta G^\circ = -22.9$ kJ/mol) is largely driven by enthalpy ($\Delta H^\circ = -19.8$ kJ/mol) and slight entropy ($\Delta S^\circ = 10.3$ J/mol K) changes. ^{1}H NMR and MM$^+$ studies indicate formation of two isomeric 1:1 complexes: one involving complete inclusion of the phenyl-moiety into the β-CyD cavity while the other pertaining to partial inclusion of the pyrimidinone moiety. The dominant driving force for complexation is evidently van der Waals with very little electrostatic contribution. DSC, XRPD and ^{1}H NMR studies proved the formation of inclusion complex in solution and the solid state.

Keywords: Sildenafil; Cyclodextrin; Isomeric inclusion complexes; Phase solubility diagrams; DSC; ^{1}H NMR; Molecular modeling

1. Introduction

Sild, 1-{[3-(6,7-dihydro-1-methyl-7-oxo-3-propyl-1H-pyrazolo [4,3-d] pyrimidin-5-yl)-4-ethoxyphenyl] sulfonyl}-4-methylpiperazine, is used to treat male erectile dysfunction. It is a selective inhibitor of cyclic guanosine monophosphate (cGMP)-specific phosphdiesterase type 5 (PDE5). It was discovered by scientists at Pfizer and was approved by the FDA on March 27, 1998. It is available under the trademark VIAGRA in tablet dosage form containing 25, 50 and 100 mg of Sild. It is rapidly absorbed after oral administration, having a relatively low absolute bioavailability of about 40% [1].

In the literature, different patents describe methods to improve the absorption of Sild and its rate by developing a rapidly releasing pharmaceutical dosage form with low-substituted hydroxypropyl cellulose and microcrystalline cellulose [2], a nasal formulation [3,4], a fast dissolving oral dosage form [5], a microsphere [6] and a nanoparticulate composition to eliminate the effect of food on the pharmacokinetic profiles [7]. Also CyDs, mainly hydroxypropyl-β-CyD (HP-β-CyD), were used to enhance the absorption of Sild or to minimize its side effects in different formulations including sublingual or buccal tablet [8], nasal solution or colloidal dispersion [9], granule or powder for injection, capsule, tablet, etc. [10,11].

In this study, the interaction of Sild with CyDs was investigated. The contribution of the hydrophobic character of Sild to complex stability with β-CyD was determined by establishing the relationship between the K_{11} and the inherent solubility

* Corresponding author. Tel.: +962 6 4290744; fax: +962 6 4290953.
E-mail address: momari@jpm.com.jo (M.M. Al Omari).

0731-7085/$ – see front matter © 2006 Elsevier B.V. All rights reserved.
doi:10.1016/j.jpba.2006.01.055

of Sild (S_o) at different pHs. The thermodynamic parameters were also obtained to evaluate the driving forces to complex formation. In addition, DSC, XRPD, ^{1}H NMR and MM$^+$ were conducted to check whether inclusion complex formation takes place, and to explore possible guest–host interaction sites.

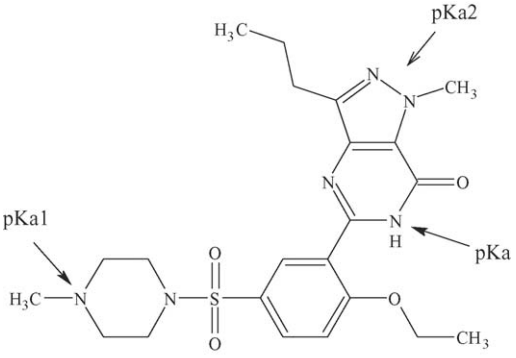

Chemical structure of Sildenafil (**Sild**)

2. Experimental

2.1. Materials

Sild citrate and CyDs (α-, β-, HP-β- and γ-CyDs) were provided by The Jordanian Pharmaceutical Manufacturing Company (JPM). The neutral form (Sild) was prepared by neutralization of Sild citrate (3 mmol), dissolved in sufficient amount of water, with 0.1 M NaOH solution, the precipitate was collected and dried at 40 °C. The hydrochloride salt of Sild and its β-CyD complex were prepared by dissolving Sild (3 mmol) in sufficient amounts of water containing equimolar amount of HCl and β-CyD. The samples were freeze-dried and the solids were collected. All other chemicals were of analytical grade obtained from Merck/Germany and Surechem/UK.

2.2. Instrumentation

UV/visible spectrophotometer (Du-650i, Beckman, USA). Thermostatic shaker (1086, GFL, Germany). pH-meter (3030, Jenway, England). Freeze dryer (Heto FD3, Heto-Holten A/S, Denmark). DSC (910S, TA instrument, USA). X-ray diffractometer (Philips PW 1729 X-ray Generator. NMR spectrometer (GSX400, JEOL, Japan).

2.3. Determination of ionization constants (pK_as)

2.3.1. By UV absorption spectrophotometry

A stock solution of Sild citrate (0.75 mM) was prepared by dissolving predetermined amounts (0.15 mmol) in 200 mL of water, which was diluted further with 0.05 M citrate buffers of different pHs ranging from 2 to 12 to obtain final solutions having fixed concentration of 0.034 mM. The absorbencies of these solutions were measured using first derivative UV/visible spectrophotometry at 310 nm. It should be noted that first derivative UV spectrophotometry was consistently used throughout this work following careful examination of absorption spectra against β-CD concentration at different pHs, which showed the absence of interferences at this wavelength.

To obtain the acid/base ionization constants of Sild, the measured absorbencies (A) at different pHs were analyzed through non-linear regression using the following equilibria:

$$HA \rightleftharpoons H^+ + A^-; \qquad K_a = \frac{(H^+)\, y\, [A^-]}{[HA]} \tag{1}$$

$$H_2A^+ \rightleftharpoons H^+ + HA; \qquad K_{a1} = \frac{(H^+)\, [HA]}{y[H_2A^+]} \tag{2}$$

$$H_3A^{2+} \rightleftharpoons H^+ + H_2A^+; \qquad K_{a2} = \frac{(H^+)\, y[H_2A^+]}{y^4\, [H_3A^{2+}]} \tag{3}$$

where HA denotes neutral Sild while H_2A^+ and H_3A^+ denote mono-and diprotonated Sild, respectively. The total concentration of Sild (C), which was kept constant at 0.034 mM, is given by:

$$C = [HA] + [A^-] + [H_2A^+] + [H_3A^{2+}] = [HA]\left\{1 + \frac{K_a}{y(H^+)} + \frac{(H^+)}{yK_{a1}} + \frac{(H^+)^2}{y^4\, K_{a1}K_{a2}}\right\} = [HA]\alpha \tag{4}$$

where

$$\alpha = 1 + \frac{K_a}{y(H^+)} + \frac{(H^+)}{yK_{a1}} + \frac{(H^+)^2}{y^4 K_{a1} K_{a2}} \tag{5}$$

$(H^+) = 10^{-pH}$ and y is the molar mean activity coefficient of ionic species given by the Davies equation: $\log y_i = -B|z^+z^-|\{\sqrt{I}/(1+\sqrt{I}) - 0.3I\}$, where $I = -1/2\sum c_i z_i^2$ and $B = 1.825 \times 10^6\, \rho^{1/2}/(\varepsilon T)^{3/2}$ while ρ and ε are, respectively, the density and dielectric constant of water at absolute temperature T.

The fractions of different Sild species (f), which vary with pH, are given by

$$f_{HA} = \frac{1}{\alpha}$$
$$f_{A^-} = \frac{K_a/y(H^+)}{\alpha}$$
$$f_{H_2A^+} = \frac{(H^+)/yK_{a1}}{\alpha} \tag{6}$$
$$f_{H_3A^{2+}} = \frac{(H^+)^2/y^4 K_{a1} K_{a2}}{\alpha}$$

Combining Eqs. (4)–(6), the predicted value of the absorbance (A^P) would be given by:

$$A^P = \{\varepsilon_{A^-}[A^-] + \varepsilon_{HA}[HA] + \varepsilon_{H_2A^+}[H_2A^+] + \varepsilon_{H_3A^{2+}}[H_3A^{2+}]\} = C\{\varepsilon_{A^-}\, f_{A^-} + \varepsilon_{HA}\, f_{HA} + \varepsilon_{H_2A^+}\, f_{H_2A^+} + \varepsilon_{H_3A^{2+}}\, f_{H_3A^{2+}}\} \tag{7}$$

where $\varepsilon_{A^-}, \varepsilon_{HA}, \varepsilon_{H_2A^+}$ and $\varepsilon_{H_3A^{2+}}$ are the molar absorptivities of A^-, HA, H_2A^+ and H_3A^{2+}, respectively. Non-linear regression of A against pH, with the molar absorptivities and K_as used as floating parameters, yields the best estimates of K_a, K_{a1} and K_{a2} by minimizing the function $SSE = \sum(A^P - A)^2$.

2.3.2. By pH solubility profile

Excess amounts of Sild (200 mg) were added to 50 mL of 0.05 M citrate buffers with pH ranging from 2 to 12. The samples were mechanically shaken in a thermostatic bath shaker at 30 °C to attain equilibrium (2 days), an aliquot was filtered using a 0.45 μm filter (cellulose acetate or cellulose nitrate, Advantec MFS Inc., Duplin, USA). The Sild content was determined using first derivative UV spectrophotometry at 310 nm.

Referring to the acid/base equilibria of Sild indicated in Eqs. (1)–(3) above, estimates of the ionization constants of Sild and the solubility product (K_{sp}) of the corresponding citrate salt were obtained by non-linear regression of the measured inherent solubility (S_o) of Sild against pH according to:

$$S_o = [HA] + [A^-] + [H_2A^+] + [H_3A^{2+}] = [HA]\left\{1 + \frac{K_a}{y(H^+)} + \frac{(H^+)}{yK_{a1}} + \frac{(H^+)^2}{y^4K_{a1}K_{a2}}\right\} \quad (8)$$

or

$$S_o = [HA]\left\{1 + \frac{K_a}{y(H^+)} + \frac{K_{sp}}{y^2[citrate^{-1}]} + \frac{(H^+)^2}{y^4K_{a1}K_{a2}}\right\} \quad (9)$$

Eq. (8) was automatically switched into Eq. (9) in the pH region where S_o was limited by saturation of the SildH^+·citrate^{-1} salt (pH < 4.2). No salt saturation was observed for the diprotonated Sild species (H_3A^{2+}) because its pK_{a2} value was found much lower than zero. Best estimates for K_{11} and K_{12} were obtained by minimizing the function SSE = $\sum(S_o^P - S_o)^2$ where S_o^P is the predicted value of S_o.

2.4. Phase solubility studies

Solubility studies were performed as described earlier [12]. Excess amounts of Sild (200 mg) were added to 50 mL of the desired aqueous CyD solutions ranging in concentration from 0 to 16 mM. The samples were mechanically shaken in a thermostatic bath shaker to attain equilibrium (2 days), an aliquot was filtered using a 0.45 μm filter. The pH of the filtrate was measured by calibrated pH-meter. The Sild content was determined using the same methods described above in the pH solubility profile study.

Phase solubility diagrams were analyzed to obtain estimates of the complex formation constants of soluble complexes following rigorous procedures described earlier [13]. By assuming the formation of 1:1 (SL) and 1:2 (SL_2) soluble Sild/CyD complexes, the individual complex formation constants of SL and SL_2 complexes defined as K_{11} and K_{12} are given by:

$$K_{11} = \frac{[SL]}{[S][L]} \quad (10)$$

$$K_{12} = \frac{[SL_2]}{[SL][L]} \quad (11)$$

The solubility (S_{eq}) of Sild in aqueous CyD solutions of variable concentrations is given by:

$$S_{eq} = [S] + [SL] + [SL_2] = [S] + K_{11}[S][L] + K_{11}K_{12}[S][L]^2 \quad (12)$$

where [S] and [L] donate the concentrations of free Sild and CyD, respectively. Since the solutions are saturated with Sild [S] = S_o which is the solubility of Sild at zero CyD concentration, while [SL] and [SL_2] represent the concentrations of 1:1 and 1:2 Sild/CyD complexes, respectively, Eq. (12) reduces to

$$S_{eq} = S_o + K_{11}S_o[L] + K_{11}K_{12}S_o[L]^2 \quad (13)$$

The value of [L] was estimated from the total concentration of CyD in solution (L_{eq}) given by:

$$L_{eq} = [L] + [SL] + 2[SL_2] = [L] + K_{11}S_o[L] + 2K_{11}K_{12}S_o[L]^2 \quad (14)$$

and thus

$$[L] = \frac{-b + (b^2 + aL_{eq})^{1/2}}{2a} \quad (15)$$

where

$$a = 2K_{11}K_{12}S_o \text{ and } b = 1 + K_{11}S_o \quad (16)$$

Non-linear regression of experimental data corresponding to each phase diagram was conducted to obtain the best estimates of S_o, K_{11} and K_{12} by minimizing the sum of squares of errors given by:

$$SSE = \sum (S_{eq}^P - S_{eq})^2 \quad (17)$$

where S_{eq}^P is the predicted equilibrium solubility of Sild. The results of rigorous analysis indicated only the formation of only SL soluble complex and no SL_2 type complex within the limits of experimental error ($K_{12} < 0.01\ M^{-1}$).

2.5. Non-linear regression of experimental data

Rigorous non-linear regression of experimental data was conducted using the Marquardt–Levenberg finite difference algorithm utilized by the SPSS statistical package (SPSS 10.0 for Windows Statistical Package, SPSS Inc., 233 S. Wacker Drive, Chicago, Illinois), and data plots were linked to Microsoft Excel for reproduction.

2.6. Estimation of thermodynamic parameters

Gibbs and Van't Hoff equations were used to estimate the thermodynamic parameters ΔH°, ΔS° and ΔG° according to:

$$\Delta G^\circ = \Delta H^\circ - T\,\Delta S^\circ \quad (18)$$

$$\ln(K) = \frac{\Delta S^\circ}{R} - \frac{\Delta H^\circ}{RT} \quad (19)$$

A plot of ln (K) versus 1/T produces:
Slope = $-\Delta H^\circ/R$ and intercept = $\Delta S^\circ/R$

K above stands for either K_{11}^x or S_o^x, where x denotes the mole fraction standard state (the values of K_{11} and S_o, which were initially obtained in molar concentration units, were converted to the dimensionless mole fraction units K_{11}^x and S_o^x).

2.7. ^1H NMR spectroscopy

Samples were dissolved in 99.98% D_2O and filtered before use. ^1H NMR spectra were obtained at 400 MHz and 25 °C. Chemical shifts are quoted relative to sodium 3-trimethylsilyl [D_4] propionate at 0.0 ppm, but spectra were calibrated via the known position of the residual HOD resonance, which was used as a reference.

2.8. Differential scanning calorimetry (DSC)

The thermal behaviors of Sild·HCl, β-CyD, a physical mixture of Sild·HCl and β-CyD and Sild·HCl/β-CyD complex were studied by separately heating an accurately weighed sample of each equivalent to 5 mg Sild·HCl in a sealed aluminum pan, using an empty pan sealed as reference, over the temperature range of 30–300 °C, at a rate of 10 °C/min. Indium standard was used for calibrating the temperature.

2.9. X-ray powder diffractiometry (XRPD)

The XRPD patterns were measured with X-ray diffractometer. Radiations generated from Co Kα source and filtered through Ni filters with a wavelength of 1.79025 Å at 40 mA and 35 kV were used. The instrument was operated over the 2θ range of 5–55°.

2.10. Molecular modeling

Molecular mechanical modeling was performed by MM^+ force field using HyperChem6 software (Hypercube, Canada) as described earlier [14]. The geometrical structures of Sild [15] and β-CyD [16] were separately optimized again using the Amber force field by imposing a restraint on the dihedral angles to the average values [17]. The energetics of interaction were simulated in vacuum, where water molecules were ignored to save computational time especially for large molecules [18]. The previously optimized structures of Sild and β-CyD molecules were allowed to approach each other along the symmetric axis (the x-axis) passing through the center of the β-CyD cavity. Interaction energies were computed for the drug approaching from its methylpiperazine group through the wide and narrow rims of β-CyD cavity to access the most probable optimal configurations for the complex formed. The binding energy $E_{binding}$ ($E_{complex} - \sum E_{components}$) was plotted against x for each longitudinal approach to indicate the energy minima. The binding energies ($E_{binding}$) corresponding to energy minima were computed together with their electrostatic and van der Waals contributions.

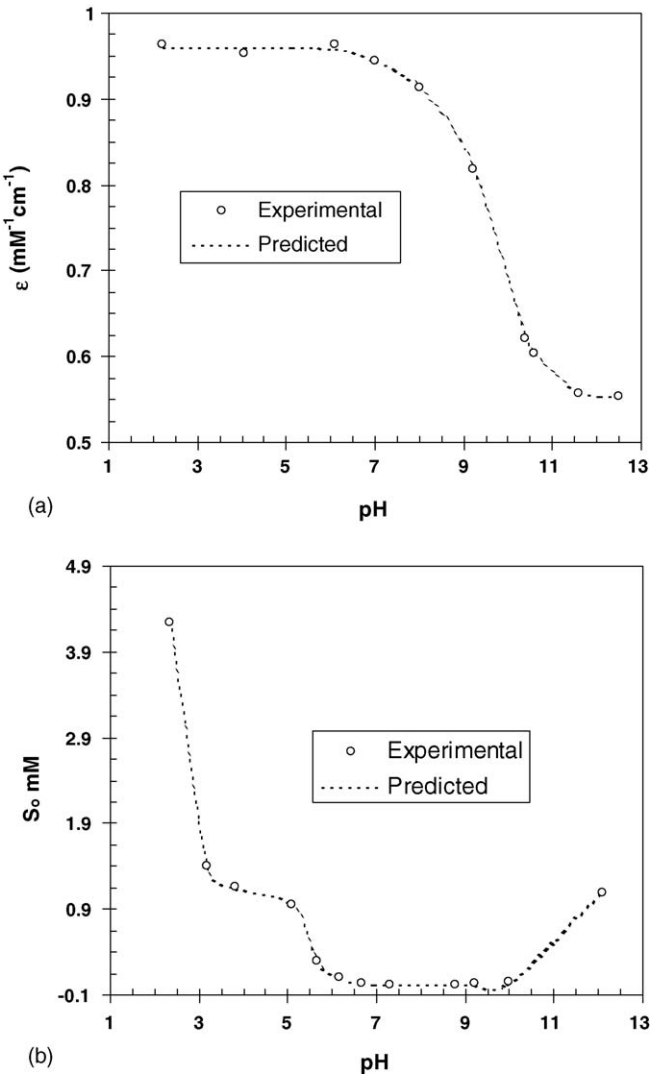

Fig. 1. Plots of the variation of: (a) the absorbance of a fixed concentration of Sild (0.034 mM) at 310 nm, and (b) the inherent solubility of Sild (S_o) against pH, both measured in 0.05 M citrate buffer at 30 °C.

3. Results and discussion

3.1. Ionization constants (pK_as)

Analysis of the variation of the first derivative UV absorptivity of a fixed concentration of Sild (0.034 mM) at 310 nm with pH (Fig. 1a) according to Eq. (7) yielded the values: $pK_a = 9.84$, $pK_{a1} = 7.10$ and $pK_{a2} < 0$. The corresponding analysis of the variation of inherent solubility (S_o) with pH (Fig. 1b) according to Eqs. (8) and (9) yielded: $pK_a = 10.3$, $pK_{a1} = 7.10$ and $pK_{a2} < 0$. The discrepancy in the value of pK_a obtained by the UV spectrophotometric method (9.84) at fixed Sild concentration from that of the pH solubility profile (10.3) is obviously due to the difficulty of controlling pH for the saturated solution above pH 9 in the latter method. Therefore the pK_a value corresponding to acid ionization of the pyrimidinone moiety obtained at $pK_a = 9.84$ is more accurate. Both methods yield a pK_{a1} value of 7.10 corresponding to the basic ionization of the piperazine moiety. The solubility product of the $SildH^+ \cdot citrate^{-1}$ salt was estimated

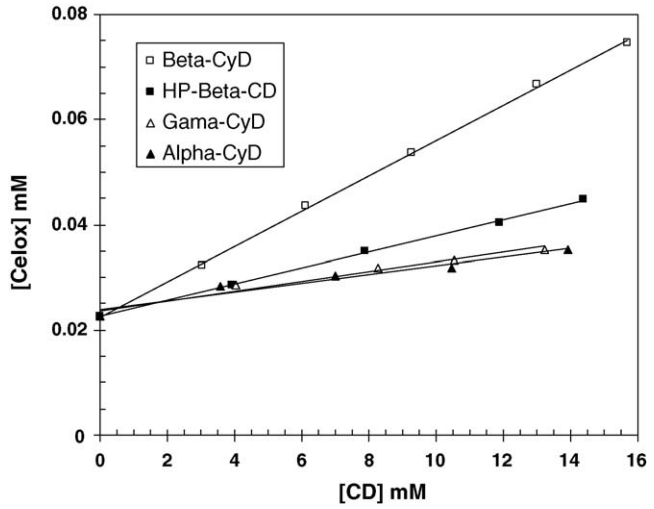

Fig. 2. Phase solubility diagrams of the Sild/CyD systems obtained in 0.05 M citrate buffer at pH 8.7 and 30 °C.

at $pK_{sp} = 1.53$. Earlier studies involving potentiometric titrations of aqueous methanol solutions of Sild reported $pK_a = 9.12$ and $pK_{a1} = 6.78$ [15]. We believe that values of $pK_a = 9.84$ and $pK_{a1} = 7.10$ are more accurate because of the expected errors inherent to extrapolation of titration results conducted in aqueous organic solutions. Another work reported a basic pK_{a1} value of 8.7, but the method of pK_{a1} determination was not stated [19] and therefore could not be evaluated here.

3.2. Effect of CyD type

Fig. 2 depicts PSDs obtained for Sild against each of α-, β-, HP-β- and γ-CyD concentration in 0.05 M citrate buffers (pH 8.7) and 30 °C. At this pH, Sild predominantly exists as a neutral molecule with an inherent solubility (S_o) of 0.023 mM. The K_{11} values were 150, 68, 46 and 43 M^{-1} for β-CyD, HP-β-CyD, γ-CyD and α-CyD, respectively (Table 1). The low K_{11} values in case of α-CyD, HP-β-CyD and γ-CyD are most likely due to two factors: (a) they are highly soluble in water thus lowering the driving force to complex with Sild, and (b) α-CyD has a small cavity size that reduces the probability of including the bulky groups of Sild, while γ-CyD has a large cavity size thus lowering effective interactions with Sild [14,20]. The binding of Sild with HP-β-CyD is relatively less than that with β-CyD, probably due to the presence of substituent hydroxypropyl groups at the rims of the-β-CyD cavity in HP-β-CyD, which may retard the inclusion of Sild via steric hindrance [21].

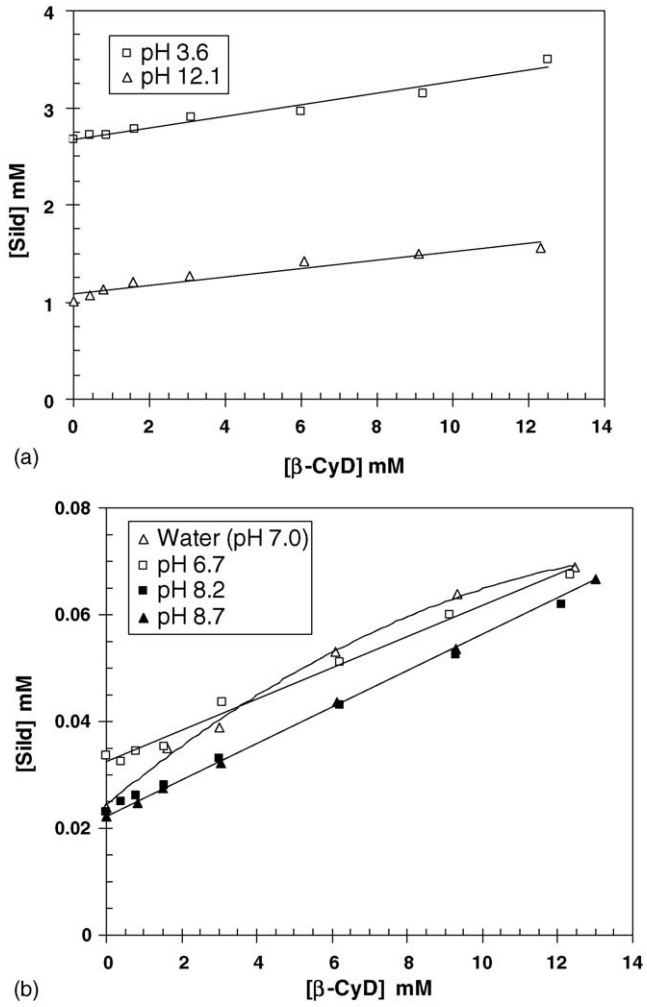

Fig. 3. Phase solubility diagrams of the Sild/β-CyD system in water (pH 7.0) and in 0.05 M citrate buffers of different pHs: (a) at pHs 3.6 and 12.1 and (b) at pHs 6.7 and 8.7 at 30 °C.

3.3. Effect of pH on complex formation complex (K_{11})

The PSDs obtained in water and in 0.05 M citrate buffer of different pHs are shown in Fig. 3. The corresponding K_{11} values are listed in Table 2. The result at pH 8.7, where Sild is predominantly neutral, indicates that the K_{11} values are relatively high

Table 1
Complex formation parameters for Sild/CyD systems in 0.05 M citrate buffer at pH 8.7 and 30 °C

CyD	Phase solubility diagram type	K_{11} (M^{-1})	EF
β-CyD	A_L	150 (±5)	3.2
HP-β-CyD	A_L	68 (±4)	2.0
γ-CyD	A_L	46 (±19)	1.6
α-CyD	A_L	43 (±20)	1.6

The enhancement factor (EF) = S_{eq}/S_o, where S_{eq} and S_o are the solubilities of Sild in the presence (15 mM) and absence of CyD, respectively.

Table 2
Estimates of complex formation constants (K_{11}) for the Sild/β-CyD system obtained in water and in 0.05 M citrate buffer at different pHs and 30 °C

pH	S_o (mM)	K_{11} (M^{-1})
Water (pH 7.0)	0.024 (±0.004)	170 (±30)
3.6	2.67 (±0.07)	17 (±4)
6.7	0.0335 (±0.002)	85 (±10)
8.2	0.0230 (±0.001)	140 (±4)
8.7	0.0223 (±0.001)	150 (±5)
12.1	1.12 (±0.04)	42 (±8)

S_o is the solubility of Sild in the absence of β-CyD.

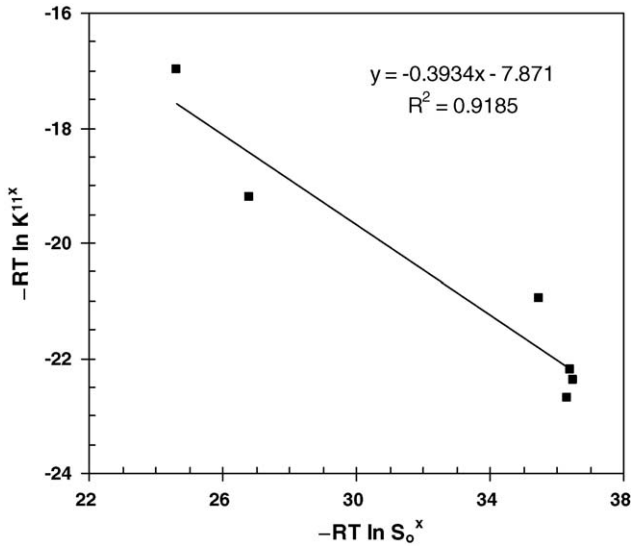

Fig. 4. A plot of $-RT\ln K_{11}^{x}$ against $-RT\ln S_{o}^{x}$ for the data in Table 2 (x denotes the mole fraction standard state).

($150\,M^{-1}$), while they are lower for ionized Sild at pHs 3.6 and 12.1 (17 and $42\,M^{-1}$), where it exists as protonated and anionic species, respectively.

Different parameters were used earlier to identify possible correlation between the strength of binding and the hydrophobic effect, including the partition coefficient, hydrophobic surface area, number of carbon atoms of a homologous series of substrates, and the addition of organic co-solvents and salts to the media [22].

In this work, a quantitative measure of the contribution of the hydrophobic effect (desolvation) to complex formation was obtained from possible correlation of the free energy of complex formation ($\Delta G_{11} = -RT\ln K_{11}^{x}$) with the free energy of inherent Sild solubility ($\Delta G_{S_o} = -RT\ln S_{o}^{x}$) obtained in 0.05 M citrate buffer of different pHs (x depicts the mole fraction standard state, where the units of K_{11} (M^{-1}) and S_o (M) are transformed to mole fraction units by multiplying K_{11} with 55.5 and dividing S_o by 55.5, respectively (55.5 represents the number of moles of water in 1 L dilute aqueous solution). For example, if ΔG_{11} varies linearly with ΔG_{S_o}, then the negative slope of the linear plot would indicate the contribution of the hydrophobic character of Sild towards complex formation. On the other hand, the intercept would provide a measure of the contribution of other factors, including specific interactions, to complex stability [23].

The extent to which complex formation is influenced by the hydrophobic effect is depicted in Fig. 4. The linear variation of $\ln K_{11}^{x}$ against $\ln S_{o}^{x}$ for all data listed in Table 2 indicates that almost 39% of the tendency for complex formation is driven by the hydrophobic character of Sild (desolvation), while other factors including specific interactions constitute about −7.9 kJ/mol.

3.4. Thermodynamics

The PSDs of Sild obtained in 0.05 M citrate buffer (pH 8.7) at different temperatures are shown in Fig. 5a. The corresponding complex formation constants (K_{11}) and the solubilities of Sild

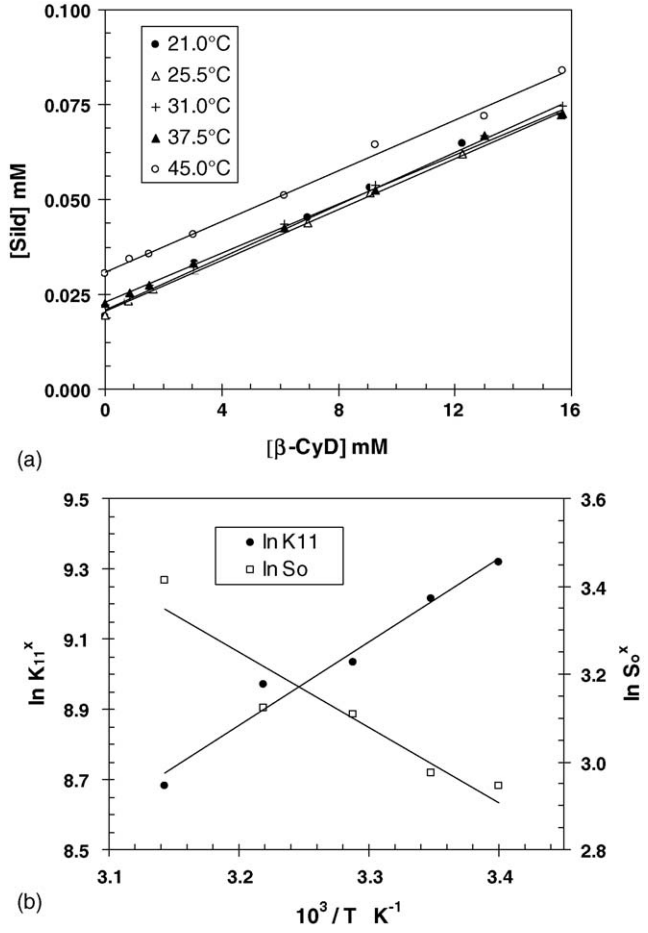

Fig. 5. (a) Phase solubility diagrams of the Sild/β-CyD system in 0.05 M citrate buffer (pH 8.7) at different temperatures and (b) plots of $\ln K_{11}^{x}$ and $\ln S_{o}^{x}$ against $1/T$ (x denotes the mole fraction standard state).

in the absence of β-CyD (S_o) are listed in Table 3. Van't Hoff plots of $\ln K_{11}^{x}$ and $\ln S_{o}^{x}$ against $1/T$ are shown in Fig. 5b, while the thermodynamic parameters (ΔH°, ΔS° and ΔG°) are listed in Table 3.

The results suggest that complex formation for Sild ($\Delta G^{\circ} = -22.9$ kJ/mol) is largely driven by enthalpy ($\Delta H^{\circ} = -19.8$ kJ/mol) and slight entropy ($\Delta S^{\circ} = 10.3$ J/mol K))

Table 3
Estimates of complex formation constants (K_{11}) of the Sild/β-CyD system obtained in 0.05 M citrate buffer at pH 8.7 and different temperatures, and the thermodynamic parameters corresponding to inherent Sild solubility (S_o obtained in the absence of β-CyD) and complex formation constant (K_{11}) obtained from Van't Hoff plots

T (°C)	S_o (mM)	K_{11} (M^{-1})
21.0	0.0190 (±0.002)	201 (±23)
25.5	0.0196 (±0.001)	180 (±9)
31.0	0.0223 (±0.001)	150 (±5)
37.5	0.0227 (±0.001)	143 (±7)
45.0	0.0303 (±0.002)	111 (±11)

	ΔG° (kJ/mol)	ΔH° (kJ/mol)	ΔS° (J/mol K)
Solubility of Sild (S_o)	36.8 (±9.2)	14.3 (±9.2)	−75.5 (±30.8)
Sild/β-CyD complex	−22.9 (±6.6)	−19.8 (±6.6)	10.3 (±22.3)

changes, which are attributed to van der Waals interaction and solvent disordering [24]. While the solubility of Sild (S_o) is impeded both by enthalpy ($\Delta H^\circ = 14.3$ kJ/mol) and relatively large entropy ($\Delta S^\circ = -75.5$ J/mol K) changes.

3.5. ^{1}H-nuclear magnetic resonance

^{1}H NMR spectra of Sild·HCl, β-CyD and the Sild·HCl/β-CyD complex are shown in Fig. 6, while their corresponding proton assignments are listed in Table 4. Inspection of the table shows that the upfield chemical shift displacement ($\Delta\delta$) on complexation are highest for protons H_3 (−0.010 ppm) and H_5 (−0.033 ppm) of β-CyD. This indicates that the inclusion of Sild into the β-CyD cavity, especially since these two protons are located inside the cavity [25]. Other protons H_1, H_2, H_4 and $H_{6,6'}$ demonstrate less significant $\Delta\delta$ (−0.003 to −0.006 ppm) on complexation. As to Sild, protons III, IV, VI, *a* and *b* exhibit the highest downfield displacements ($\Delta\delta = 0.013$–0.020 ppm), which indicate possible inclusion of the pyrimidinone- and phenyl-moieties and thus formation of isomeric 1:1 complexes. The methylpiperazine group appears to be situated mostly outside of the cavity as is indicated by the relatively low $\Delta\delta$ values of protons VII, VIII and IX.

3.6. Differential scanning calorimetry

DSC thermograms of Sild·HCl, β-CyD, a physical mixture of Sild·HCl and β-CyD and the Sild·HCl/β-CyD complex are shown in Fig. 7. Sild·HCl has an endothermic peak at about 226 °C. This peak was retained in the physical mixture of Sild·HCl and β-CyD, while it almost disappeared in the thermogram of the complex indicating that Sild·HCl/β-CyD is an inclusion complex.

3.7. X-ray powder diffractiometry (XRPD)

The XRPD patterns of Sild·HCl, β-CyD, a physical mixture of Sild·HCl and β-CyD, and the Sild·HCl/β-CyD complex are

Table 4
The 400 MHz ^{1}H NMR chemical shifts (δ in ppm) of (-CyD, Sild·HCl and the Sild·HCl/(-CyD complex and the corresponding chemical shift displacements ($\Delta\delta = \delta_{complex} - \delta_{component}$) obtained in D_2O at 25 °C (n_H denotes the number of protons)

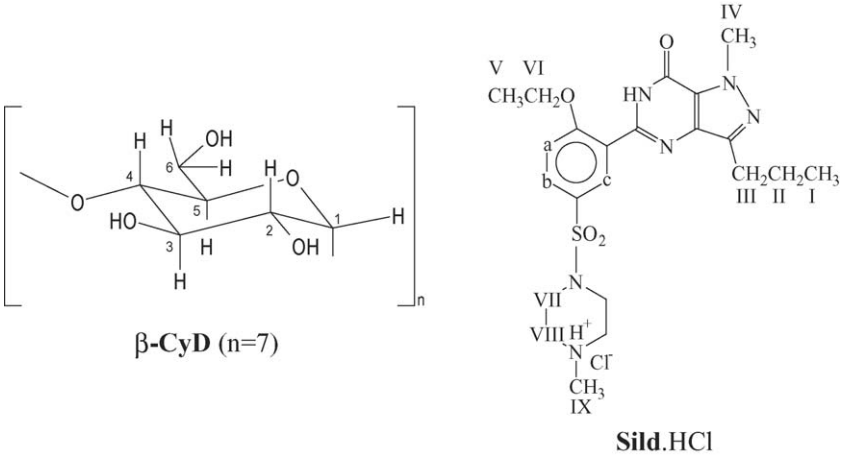

Assignment	n_H	Multiplicity	δ	$\delta_{Complex}$	$\Delta\delta_{ppm}$
β-CyD					
H_2, H_4, $H_{6,6'}$	28	Triplet	3.594	3.590	−0.003 to −0.006
H_5	7	Triplet	3.889	3.856	−0.033
H_3	7	Triplet	3.976	3.966	−0.010
H_1	7	Doublet	5.082	5.076	−0.006
Sild·HCl					
I	3	Triplet	0.916	0.920	0.004
V	3	Triplet	1.458	1.461	0.003
II	2	Multiplet	1.706	1.712	0.006
III	2	Triplet	2.773	2.789	0.016
VIII (ax)	2	Multiplet	2.873	2.876	0.003
IX	3	Singlet	2.919	2.920	0.001
VII (ax)	2	Multiplet	3.263	3.265	0.002
VIII (eq)	2	Multiplet	3.620	Interferes with β-CD	
VII (eq)	2	Multiplet	3.926	Interferes with β-CD	
IV	3	Singlet	4.137	4.157	0.020
VI	2	Quartet	4.273	4.286	0.013
a	1	Doublet	7.317	7.327	0.010
b	1	Multiplet	7.909	7.925	0.016
c	1	Doublet	8.086	8.083	−0.003

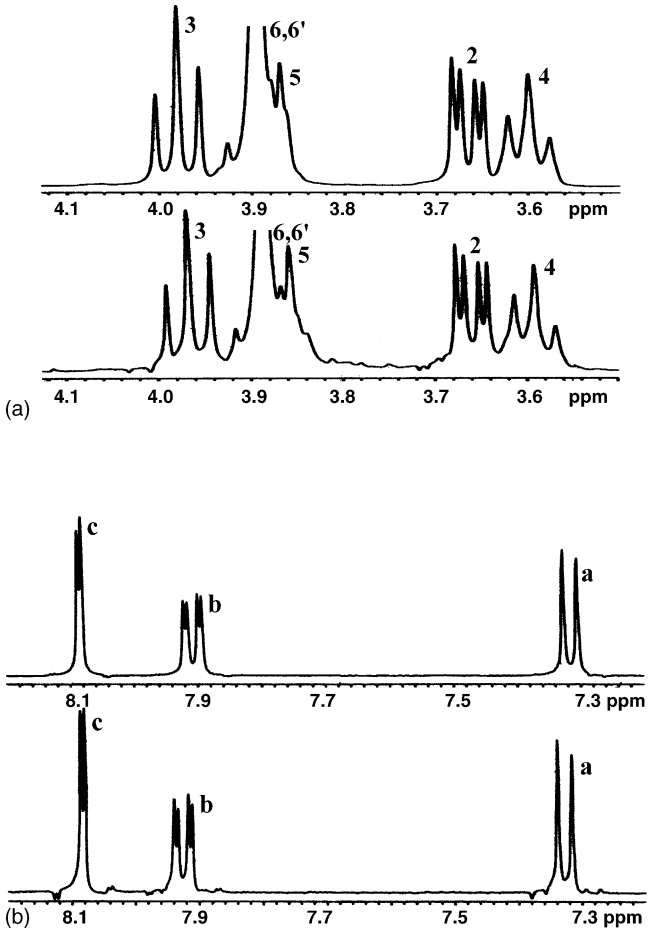

Fig. 6. ^{1}H NMR spectra of the Sild·HCl/β-CyD system in D_2O at 25 °C: (a) for protons of β-CD and (b) for aromatic protons of Sild·HCl. The upper and lower traces correspond to the compound before and after complexation, respectively.

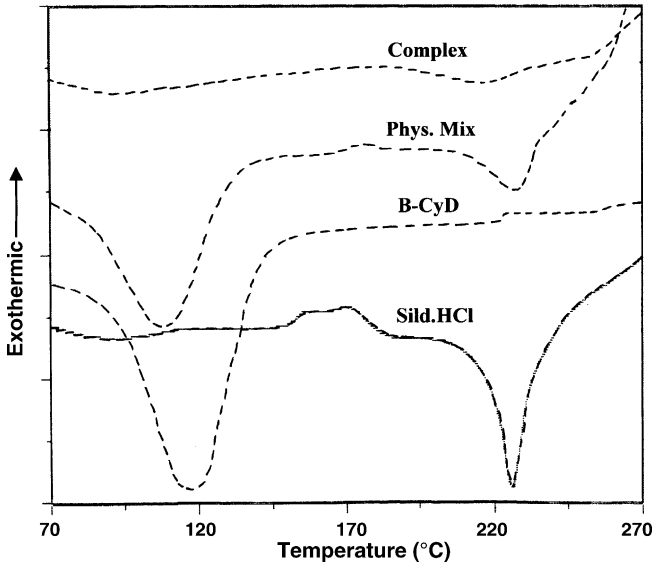

Fig. 7. DSC thermograms of Sild·HCl, β-CyD, Sild·HCl/β-CyD, a physical mixture of Sild·HCl and β-CyD, and the Sild·HCl/β-CyD complex.

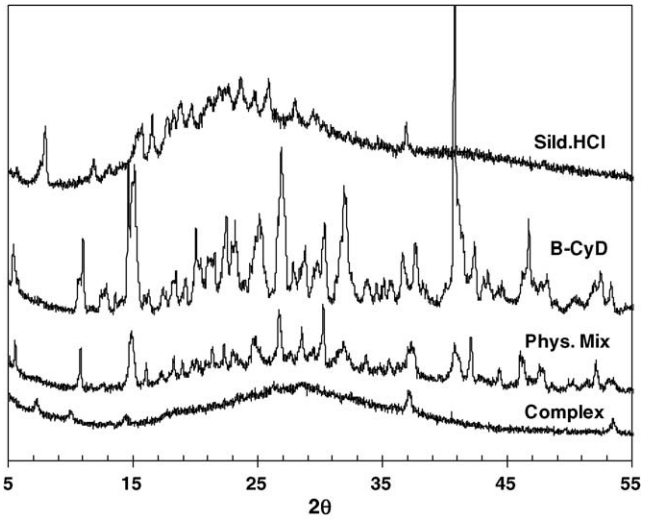

Fig. 8. XRPD patterns of Sild·HCl, β-CyD, Sild·HCl/β-CyD, a physical mixture of Sild·HCl and β-CyD, and the Sild·HCl/β-CyD complex.

presented in Fig. 8. The diffraction pattern of Sild·HCl/β-CyD complex was devoid of diffraction peaks except for a broad band centered at $2\theta = 27°$, which suggests the formation of an inclusion complex in the solid state.

3.8. Molecular modeling

The binding energies ($E_{binding}$) with their electrostatic and van der Waals contributions are listed in Table 5. The dominant driving force for complexation is evidently van der Waals with very little electrostatic contribution. The methylpiperazine approach through the wide and narrow rims proved to be the most energetically favorable route towards inclusion of Sild into the β-CyD cavity leading to complete inclusion of the phenyl group leaving the ethoxy substituent situated outside of the cavity (Fig. 9a). Further penetration yields another almost equally probable isomeric complex in which the pyrimidinone moiety is included while the ethoxyphenyl and methylpiperazine protrude

Table 5
Molecular modeling results of interaction energies ($E_{binding}$ in kcal/mol) of the two optimal configurations of Sild/β-CyD inclusion complexes (1:1) obtained for the methypiperazine approach through the wide and narrow rims of β-CyD, and the corresponding van der Waals (E_{vdw}) and electrostatic ($E_{electrostatic}$) contributions

Approach	Included moiety	$E_{binding}$	E_{vdw}	$E_{electrostatic}$
Wide rim	Phenyl	−39.0	−35.6	−3.4
	Pyrimidinone	−38.6	−32.2	−6.4
	Methylpiperazine	−34.5	−31.6	−2.9
	Pyrazole and pyrimidinone (partial)	−31.4	−26.8	−4.6
Narrow rim	Phenyl	−34.6	−34.1	−0.5
	Pyrimidinone	−33.7	−32.0	−1.7
	Methylpiperazine	−31.4	−30.7	−0.6
	Pyrazole and pyrimidinone (partial)	−29.4	−25.4	−4.0

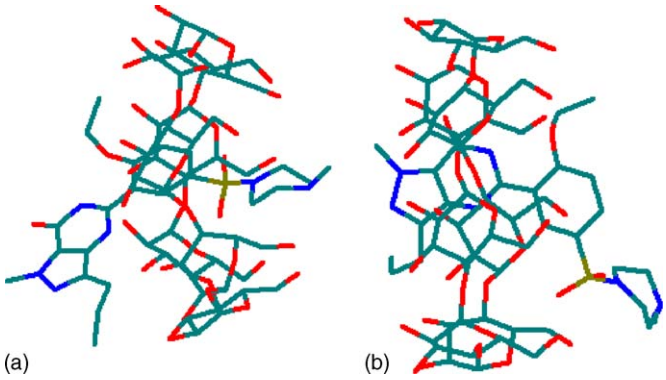

Fig. 9. Side views of the two most probable 1:1 Sild/β-CyD isomeric inclusion complex configurations obtained for: (a) inclusion of phenyl and (b) inclusion of pyrimidinone moieties.

outside of the cavity (Fig. 9b). The presence of the propyl substituent prohibits approach of the pyrimidinone moiety to either rim as an alternative direct route to complex formation. This corroborates ^{1}H NMR chemical shift displacements observed in Table 4, and thus Fig. 9a and b do simulate the most probable isomeric configuration of 1:1 Sild/β-CyD complex.

4. Conclusion

The results of this study on Sild/β-CyD complexation under different conditions reveal the following. Having an acidic (pyrimidinone) and a basic (piperazine) moieties, Sild behaves as an ampholyte, which pH solubility profile shows an increase in the solubility above pH 10 and below pH 6. The relatively high K_{11} values for β-CyD indicate the existence of a better geometric fit than with α- or γ-CyD cavities. Moreover, the higher inherent solubilities of α-, HP-β- and γ-CyD in water tend to lower their affinities to hydrophobic substrates. Ionization of Sild at low and high pHs reduces its tendency to complex, since neutral Sild forms a more stable complex. The hydrophobic character of Sild constitutes 39% of the driving force for Sild/β-CyD complex stabilization, while other factors including specific interactions contribute about −7.9 kJ/mol. Also Sild/β-CyD complex formation is favored by large enthalpic and slight entropic changes.

All the data obtained from the PSDs, DSC, XRPD, ^{1}H NMR and MM$^+$ indicated the formation of inclusion complex between Sild and β-CyD in solution and the solid state.

Acknowledgments

The authors are grateful to Dr. Tom Huckerby from Lancaster University (UK) for conducting ^{1}H NMR studies and for technical support. We are also grateful to Dr. Musa El-Barghouthi from The Hashemite University (Jordan) for technical assistance in molecular modeling studies.

References

[1] A.A. Badwan, L. Nabulsi, M.M. Al Omari, N. Daraghmeh, M. Ashour, in: Harry G. Brittain (Ed.), Sildenafil Citrate Monograph, 27, Academic Press, New York, 2001, pp. 339–376.
[2] A. Itoh, T. Niwa, Patent No. WO9,830,209, Application No. WO1997IB01471 19971120, 1998.
[3] A. Billotte, P.J. Dunn, B.T. Henry, P.V. Marshall, J.J. Woods, Patent No. EP0,967,214, Application No. EP19990304425 19990608, 1999.
[4] A.A. Hussain, L.W. Dittert, Patent No. US6,200,591, Application No. 09/208,439, 2001.
[5] W. Tian, J. Langridge, Patent No. WO2,004/017,976, Application No. PCT/GB2003/003636, 2004.
[6] F. Vaghefi, M.F. Savitzky, Patent No. US6,849,271, Application No. 274225, 2005.
[7] T.A. Ryde, D.C. Hovey, H.W. Bosch, Patent No. US20,050,042,177, Application No. US20040895405 20040721, 2005.
[8] R. El-Rashidy, Patent No. US6,087,362, Application No. 09/270,035, 2000.
[9] R.R. Vallabhaneni, Patent No. WO01/35926, Application No. PCT/IN00/00105, 2001.
[10] Y. Liu, X. Liu, W. Liu, T. Liu, Patent No. CN1,379,047, Application No. CN 2002-116766, 2002.
[11] Y. Liu, X. Liu, W. Liu, T. Liu, Patent No. EP1,514,877, Application No. 037298.3, 2005.
[12] T. Higuchi, K.A. Connors, Adv. Anal. Chem. Instr., in: C.N. Reilley (Ed.), Phase Solubility Techniques, Wiley-Intersciences, New York, 1965, pp. 117–212.
[13] M.B. Zughul, A.A. Badwan, J. Incl. Phenom. 31 (1998) 243–264.
[14] J. Taraszewska, K. Migut, M. Kozbiat, J. Phys. Org. Chem. 16 (2003) 121–126.
[15] V. Gobry, G. Bouchard, P. Carrupt, B. Testa, H. Girault, Helv. Chim. Acta. 83 (2000) 1465–1474.
[16] K. Lindner, W. Saenger, Carbohydr. Res. 99 (1982) 103–115.
[17] W. Saenger, J. Jacob, K. Gessler, T. Steiner, D. Hoffman, H. Sanbe, K. Koizumi, S.M. Smith, T. Takaha, Chem. Rev. 98 (1998) 1787.
[18] W. Tong, J.L. Lach, T. Chin, J.K. Guillory, Pharm. Res. 8 (1991) 1307–1312.
[19] J.D.H. Cooper, D.C. Muirhead, J.E. Taylor, P.R. Baker, J. Chromatogr. B. 701 (1997) 87–95.
[20] B.N. Nalluri, K.P.R. Chowdary, K.V.R. Murthy, A.R. Hayman, G. Becket. AAPS PharmSciTech. 4 (1) (2003) Article 2 (http://www.pharmscitech.org).
[21] L. Ribeiro, F. Veiga, J. Incl. Phenom. 44 (2002) 251–256.
[22] L. Liu, Q.-X. Guo, J. Incl. Phenom. 42 (2002) 1–14.
[23] M.I. El-Barghouthi, N.A. Masoud, J.K. Al-Kafawein, M.B. Zughul, A.A. Badwan, J. Incl. Phenom. 53 (2005) 15–22.
[24] C.A. Ventura, I. Giannone, D. Paolino, V. Pistara, A. Corsaro, G. Puglisi, Eur. J. Med. Chem. 40 (2005) 624–631.
[25] K.A. Connors, Chem. Rev. 97 (1997) 1325–1357.